Urban Climate 56 (2024) 102008

Contents lists available at ScienceDirect

Urban Climate

journal homepage: www.elsevier.com/locate/uclim

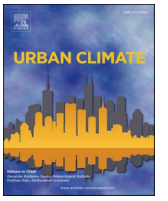

# Surface energy balance in a suburban area of the megacity of São Paulo - Seasonal variation and closure

Mauricio Jonas Ferreira [a,*], Amauri Pereira de Oliveira [a], Lucas Cardoso da Silveira [a], Georgia Codato [a], Adalgiza Fornaro [a], Agnès Borbon [b]

[a] *Laboratory of Micrometeorology, Department of Atmospheric Sciences, Institute of Astronomy, Geophysics and Atmospheric Sciences, University of São Paulo, São Paulo, Brazil*
[b] *Laboratoire de Météorologie Physique, Clermont-Ferrand, CNRS, France*

ARTICLE INFO

*Keywords:*
Surface energy balance (SEB)
Energy balance closure (EBC)
Energy flux
Urban climate
Subtropical region

ABSTRACT

The study addressed the seasonal variation and closure of the Surface Energy Balance (SEB) in a suburban area of the Megacity of São Paulo. This area consists of a combination of buildings and vegetation classified into local climate zone typologies 5 (38.5%), 6 (26.7%), and 8 (11.2%), along with areas exclusively with vegetation representing 12.1%. The investigation is based on high-quality measurements taken during February (rainy summer) and August (dry winter) between 2013 and 2015. The greatest seasonal variation was observed in latent heat flux, reaching 64.7% for daily values and 63.9% for daytime values. The smallest was observed by sensible heat flux, reaching 20.3% and 24.1%, respectively. This suggests that seasonal variation in temperature and humidity plays a crucial role in energy distribution, generating uncertainties in the closure of the energy balance. The largest difference between energy input and output was seen in August, reaching 25% for daily values and 45% for daytime values. The gap saw in closure is consistently larger in winter. The results contributed to improving understanding of energy exchanges in the surface-canopy-atmosphere system, being essential in the development of more correct meteorological and hydrological models.

## 1. Introduction

Cities change climate locally by affecting wind speed and direction, in most of the cases reducing ventilation and low-level jets intensity (Sánchez et al., 2022), in some cases intensifying wind magnitude and inducing urban wind island (Droste et al., 2018); inducing positive (negative) anomalies of air temperature (moisture content) resulting in urban heat island (urban dry island) (Landsberg, 1981; Oke, 1982; Roth, 2007; Rizwan et al., 2008; O'Malley et al., 2015; Mohajerani et al., 2017). The presence of cities increases the height of planetary boundary layer (Grimmond et al., 2010; Ribeiro et al., 2018; Sánchez et al., 2020; Moreira et al., 2022a-b); alters the spatial distribution of cloudiness and precipitation (Shepherd, 2013; Berg et al., 2014; Hao et al., 2018); and the chemical composition of the atmosphere producing air pollution events (Coutts et al., 2010; Fallmann et al., 2016). Even though they occupy approximately 5% of the Earth surface, cities are responsible by 80% of the global emission of green-house gases, contributing to climate changes at the global scale (Fang et al., 2015).

Integrating climate and urban design across diverse topologies has become a necessity, particularly in megacities situated in less

* Corresponding author.
*E-mail address:* mjferradura@hotmail.com (M.J. Ferreira).

https://doi.org/10.1016/j.uclim.2024.102008
Received 25 March 2023; Received in revised form 7 April 2024; Accepted 13 June 2024
Available online 27 June 2024

developed regions of the planet (Cui and Chui, 2021). In recent decades, these cities have experienced substantial population growth, coupled with significant environmental degradation (Roth, 2007). Over the past decades, many experiments have been conducted in urban areas with varying land use conditions, yielding valuable insights into the diverse characteristics of Surface Energy Balance (SEB) components. Many of these observations were conducted in areas characterized by structures ranging from Compact low-rise (LCZ 3) to Large low-rise (LCZ 8), as classified by the 17 Local Climate Zones (LCZs) described by Stewart and Oke (2012). This classification involves parameterizing regions with similar land cover, structure, materials, and human activities. Additionally, each LCZ exhibits distinct features such as density, impermeable area percentage, roughness, sky view factor, coating materials, and thermal behaviour (Cui and Chui, 2021; Ferreira and Duarte, 2022). To mitigate urban effects associated with climate change, it is essential to understand the surface-canopy-atmosphere interaction. In this context, surface energy balance appears as a crucial tool for generating information about local climate conditions. This information enables the identification of thermally inadequate areas, facilitating the planning of interventions to improve their climatic suitability. For instance, it provides support for the implementation of Low Impact Development (LID) practices (Ng et al., 2012; Zhang and Chui, 2019).

Replacing natural surface covering by urban fabric has a strong impact on all components of the surface energy balance, mainly net radiation and heat stored in the urban canopy. In urban areas the available energy in the surface increases due to the anthropogenic heat and surplus of energy induced by urban partition that generates positive anomalies of temperature like urban heat island (UHI). Understanding how surface energy balance (SEB) components determine the dynamic and thermodynamic properties of the atmosphere is key issue in to setting input parameters for numerical forecasting of weather, climate, and pollution dispersion in urban areas (Christen and Vogt, 2004; Shepherd, 2013; Templeton et al., 2018; Sokhi et al., 2018). The SEB equation shows that the energy available in urban areas can be expressed as the sum of energy sinks or sources are compensated by the sum of the energy fluxes across the surfaces of the volume control element that envelops the urban interface defined by Oke (1988) as:

$$Q^{*} + Q_F - \Delta Q_S - \Delta Q_A = Q_H + Q_E \quad (1)$$

Where, Q* is the net radiation at the surface, $Q_F$ the anthropogenic heat comprising all additional energy input produced by human activities, such as energy released by vehicular, stationary, and human metabolism sources. Strongly dependent on spatial distribution of energy use (industrial, commercial, and residential areas), $Q_F$ displays diurnal, seasonal, or even weekly trends. In suburban settings $Q_F$ has small size and is often omitted when information about stationary and mobile sources are not available (Taha, 1997; Offerle et al., 2005; Shahmohamadi et al., 2011; Sailor et al., 2015). Although small, local scale values of $Q_F$ are not negligible and even for suburban areas becoming a key factor in the simulation of urban boundary layer (UBL) and UHI (Chen et al., 2009; Sailor et al., 2015; Ribeiro et al., 2018; Umezaki et al., 2020).

Turbulent fluxes of sensible ($Q_H$) and latent ($Q_E$) energy are responsible by a significant fraction of the exchange of energy between surface and planetary boundary layer (PBL). $\Delta Q_S$ is the net energy flux stored in canopy and is all the mechanisms of storage and release of energy in the urban canopy. Finally, $\Delta Q_A$ is the horizontal advection of energy in the volume corresponding to the urban canopy. On the local scale and over a homogeneous urban surface $\Delta Q_A$ contributes little to the energy balance and can be neglected. However, on a regional scale an urban region with complex topography, $\Delta Q_A$ can be significant, especially close to urban-rural borders, where temperature, wind and humidity differences can be large (Oncley et al., 2007; Foken, 2008; Cuxart et al., 2016; Mauder et al., 2020). Even though, according to Foken (2008) and Cuxart et al. (2016) the advection term is not large enough to explain the non-closure in the measured SEB.

Eq. (1) is one of the pillars that theoretically support the description of Earth's climate at any scale (micro, *meso* and macroscale).

**Table 1**
A summary of factors affecting the flux estimates using eddy-covariance technique that result in the lack of EBC described in Mauder et al. (2020). The error regarding the available energy at the surface presented in the third column was obtained from the references of previous studies indicated in the first column.

| Cause of imbalance | Problem | Error range (%) |
|---|---|---|
| **Instrument error** (Foken and Oncley, 1995; Foken, 1998; Foken, 2008; Masseroni et al., 2014; Zhou et al., 2018; Mauder et al., 2020) | Systematic error of sonic anemometer<br>Systematic error of humidity measurement<br>Systematic error of radiation measurement | 5–20 |
| | Systematic error of soil heat flux | 20–50 |
| **Data processing error** (Foken, 1998; Oncley et al., 2007; Fratini and Mauder, 2014) | Mismatch of footprint | 10–30 |
| | Systematic error of correction algorithms | 5–20 |
| | Uncertainty due to averaging operator | *NA |
| **Additional sources of energy** (Oliphant et al., 2004; Oncley et al., 2007; Foken, 2008) | Canopy heat storage | 20–50 |
| | Bio-chemical energy storage (photosynthesis) | 0.5–2.0 |
| | Potential energy of water | ≈ 0.0 |
| **Sub-mesoscale transport and secondary circulations** (Oncley et al., 2007; Leuning et al., 2012; Zhou et al., 2019; Mauder et al., 2020) | Horizontal flux divergence | 5–10 |
| | Vertical/horizontal advection | 15–20 |

* Not available.

Locally (microscale) $Q_H$, $Q_E$, $Q^*$ and $Q_F$ can be estimated using in situ measurements and inventory methods (Mauder et al., 2020). Closing SEB equation below 20% remains an insurmountable barrier in micrometeorology (Foken, 2008; Schalkwijk et al., 2016). This task is particularly difficult in urban areas where ($Q_H + Q_E$) fails quite often to account for the net available energy ($Q^* - \Delta Q_S$) (Christen and Vogt, 2004; Majozi et al., 2017; Gao et al., 2017).

In the last two decades observations show the available energy is predominantly larger than the sum of sensible and latent energy fluxes. This occurs mainly when energy fluxes are estimated with eddy-covariance method (EC). In this case $Q_H + Q_E$ can be smaller than ($Q^* - \Delta Q_S$) in as much as 20% for homogeneous and up to 30% for heterogeneous surfaces (Wilson et al., 2002; Foken et al., 2006; Foken, 2008; Masseroni et al., 2014; Zhou et al., 2018). According to literature ($Q_H + Q_E$) corresponds from 70% to 90% of the available energy at the surface ($Q^* - \Delta Q_S$) (Foken, 2008; Masseroni et al., 2014; Gao et al., 2017; Zhou et al., 2019).

The imbalance of the Energy Balance Closure (EBC) over urban areas has four causes (Table 1). The first one is linked to instrument error produced by the incorrect use of turbulence sensors and misrepresentation of distinct spatial scales when sampling different layers. The second cause is associated to data processing error, i.e., the lack of data quality control and flux corrections. The third is related with misrepresentation of other energy sources. The fourth is attributed to the unaccounted turbulent energy fluxes produced by small-scale turbulence such as sub-mesoscale transport induced by secondary circulation (wavelength $> 2$ km) filtered out by EC method (Foken, 2008; Eder et al., 2014; Masseroni et al., 2014; Zhou et al., 2019; Mauder et al., 2020).

The main goal of this work is to assess the Energy Balance Closure (EBC) by comparing turbulent energy fluxes ($Q_H + Q_E$) against the net available energy ($Q^* - \Delta Q_S$) in a suburban area of São Paulo City. The EBC will be assessed by Simple Linear Regression (SLR) which considers the slope and intercept of a regression line fitted through the dispersion diagram of output ($Q_H + Q_E$) versus input energy ($Q^* - \Delta Q_S$) or calculated through the ratio between the output and input of energy indicated by Energy Balance Ratio (EBR) as proposed by Aubinet et al. (2000) and Wilson et al. (2002).

Should be emphasized that are few works available in the literature describing the seasonal variation of SEB in the São Paulo Megacity. The analysis carried by Ferreira et al. (2013), Oliveira et al. (2020) and Torres et al. (2023) were based on in situ turbulence measurements carried out from 2009 to 2012, during short periods of time:31 days in 2009 (Ferreira et al., 2013), 20 days in 2013 (Oliveira et al., 2020) and 448 days (30 in 2009, 114 in 2010, and 304 in 2012, in Torres et al. (2023). Furthermore, Supplementary Table S1 shows that only the studies by Oliveira et al. (2020) and Torres et al. (2023) cover February and August. As will be shown in this work February and August can be used as reference months to characterize the seasonal variation between Summer (dry) and Winter seasons in São Paulo. Thus, the number of days of observation during the climatic reference of summer and winter by Torres et al. (2023) are 29 and 31 days respectively in February and August of 2012. Since Ferreira et al. (2013) data was gathered between May 7 and June 8, we can conclude that to use 84 days in February and 96 in August of hight quality data measured at IAG site between 2013 and 2015 is a significant step to characterize the seasonal variation of SEB components in the São Paulo Megacity. Besides, the quality control procedure developed by Oliveira et al. (2020) and Silveira et al. (2022) assure high quality of measurements used in this work and allow us to assure that they correspond to the inertial surface sub-layer.

The results of the seasonal variation of the SEB components and energy balance closure (EBC) contribute to enhancing the understanding of energy exchanges within the surface-canopy-atmosphere system, which is crucial for constructing more accurate meteorological and hydrological models. These models are essential for urban planning to mitigate the adverse effects of climate change and to propose nature-based actions with the purpose of improving environmental conditions.

In this work site and measurements are described in Section 2. The seasonal variation of SEB components and corresponding ratios are analysed in Section 3. SEB closure analysis is shown in Section 4 and major findings are summarized in Section 5.

## 2. Site and measurements

### 2.1. Site

The Metropolitan Region of São Paulo (MRSP) comprises an urban area of 7947 $km^2$ (GEOSAMPA, 2020), inhabited by approximately 21.3 million people, ranking it as the fourth largest urban agglomeration on the planet (Supplementary Table S2) (UN, 2018). São Paulo City is the central core of the MRSP, covering 1507 $km^2$ of land at 700 m above sea level (asl) and 60 km away from the Atlantic Ocean. With around 11.9 million inhabitants, it is considered, according to administrative boundaries, part of the large 'urban agglomeration', which, unlike cities in North America and Europe, is formed by an extensive contiguous urban area and densely distributed and verticalized cores (Duarte et al., 2015; UN, 2016, 2018; IBGE, 2018; Yang et al., 2022).

#### 2.1.1. Climate

The climate of São Paulo is classified as high elevation subtropical humid (Cwb), with dry and mildly chilly winter (June–August), and wet and warm summer (December–March). In this research, the seasonal variation of air temperature, relative humidity, accumulated precipitation, wind speed and direction, are based on daily averages estimated from 5-min values of theses variables saw in the turbulence site (IAG) during February and August between 2013 and 2015. As showed in Supplementary Table S3, the MRSP climate is characterized by 80-years average values based on observations conducted from 1933 to 1990 at the PEFI climatological station located in southern São Paulo City (23°39′04"S; 46°37′20"W; 799 m asl). Belonging to the University of São Paulo, PEFI ("*Parque Estadual das Fontes do Ipiranga*") is the oldest climate station in São Paulo City with continuous observations of climatological variables since 1933. According to Ferreira et al. (2011) and Oliveira et al. (2020),

### 2.1.2. Topography

The topography was extracted from the Digital Elevation Model (DEM), built from the LiDAR 3D point cloud, with a spatial resolution of 1:1000 (accuracy of 1.0 m). The topography, considering an area of 1-km radius circle centred in the IAG (23°33′34"S; 46°44′01"W, 740 m asl), has higher elevation in the southern sectors (794 m asl) and lower in the north (719 m asl), with terrain slightly slopping toward the Pinheiros river valley to the northeast (Fig. 1a). The classification of land use was processed in the tools (toolbox), inserted in the ArcGIS v10.4.1 platform of the Environmental Systems Research Institute (ESRI) (EPC, 2020a; GEOSAMPA, 2020).

### 2.1.3. Land use and land use fraction use

In the case of IAG the land use corresponds to suburban (Supplementary Table S4; Fig. 1c). This inference is based on the land use inventory considering 6 categories proposed by Grimmond and Oke (1999). The land use was estimated within 1-km radius centred at the IAG, based on the Homogeneous Units of Use and Occupation of Urban Soil dataset of the São Paulo State from Environmental Planning Coordination (EPC, 2020a).

Land use fraction (LUF) is based on the Classification System for the Use and Standard of Urban Occupation (UHCT) through the association of different landscape elements with specific spatial patterns. This methodological approach uses the supervised classification of targets through surface sectorization in areas with similar characteristics proposed in Jog and Dixit (2016). Orthorectified images are used from the SPOT satellite (2.5-m pixel size), RapidEye satellite (5-m pixel size), and orthophoto images from the Cartographic Update Project of the São Paulo State - EMPLASA (1-m pixel size) (EPC, 2020b). The distribution of LUF in the IAG site (Fig. 1d). does also reflect the suburban character of land use (Fig. 1c). Moreover, it is key parameter to define the OHM model in Section 2.2.2.

### 2.1.4. Local climate zone

The Local Climate Zone (LCZ) classification was constructed based on measured and estimated values of geometric, thermal, radiative, metabolic, and surface cover properties gathered from urban and rural field sites worldwide (Stewart and Oke, 2012). In this work the LCZ classification was obtained from the World Urban Database and Access Portal Tool (WUDAPT) for the city of São Paulo (Bechtel and Daneke, 2012; Bechtel et al., 2015; Bechtel et al., 2019; Ferreira and Duarte, 2022). According to WUDAPT, 67.2% of the area within 1-km radius circle centred at the IAG is composed by LCZ 5 and LCZ 6 (Supplementary Table S5; Fig. 1b).

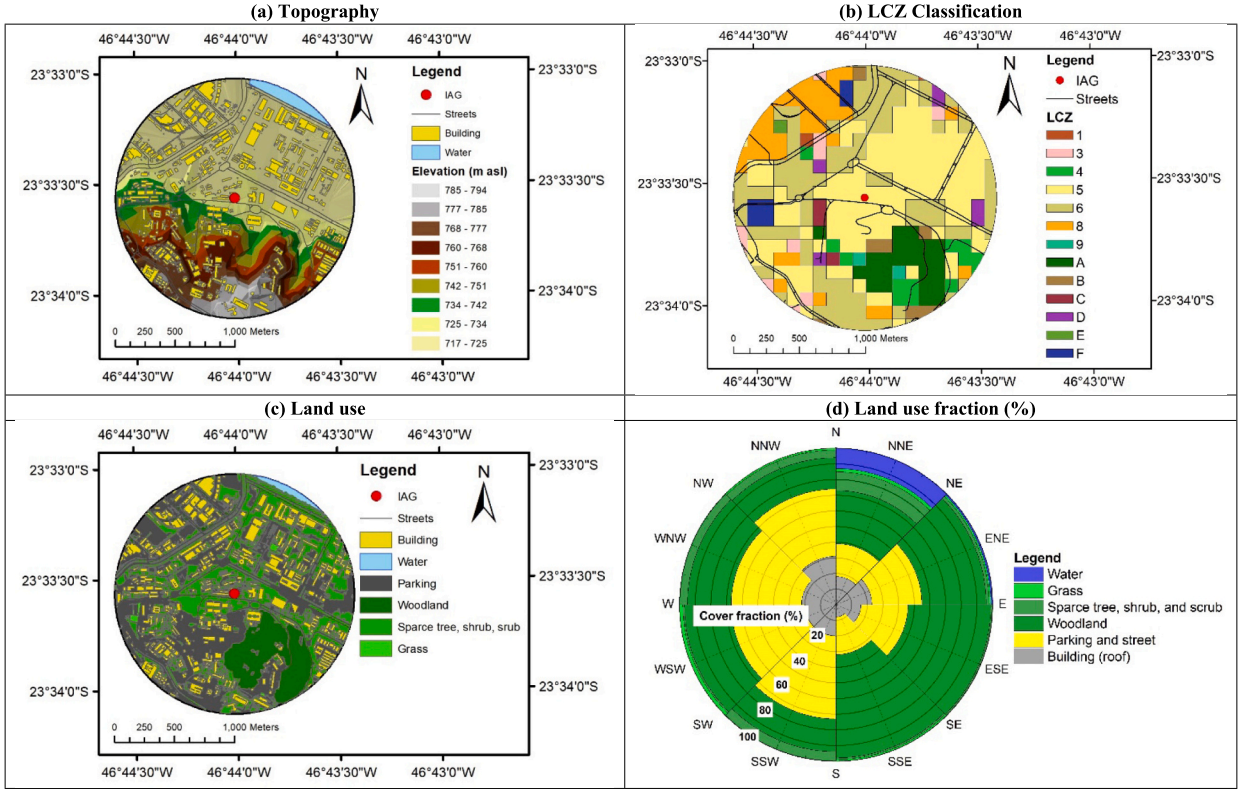


**Fig. 1.** (a) Topography, (b) LCZ, (c) Land use and (d) Land use distribution by 45°-sector in the area within 1-km radius circle centred at the IAG.

### 2.2. Measurements and empirical expressions

All measurements used in this study were conducted on a 10-m tower located in the centre of a concrete platform at 17.0 m above ground level (agl) atop a 4-story building at the Institute of Astronomy, Geophysics, and Atmospheric Sciences (IAG) on the campus of the University of São Paulo, a suburban area west of São Paulo City belonging to the observational network of three micrometeorological towers of the MCITY BRAZIL Project (Oliveira et al., 2020, Sánchez et al., 2020, Silveira et al., 2022, Sánchez et al., 2022, Moreira et al., 2022a-b), which has been expanded to four by the BIOMASP+ project, and henceforth referred to as IAG.

The SEB closure and seasonal variation analyses are based on half-hourly and hourly values of $Q_H$ and $Q_E$ estimated using eddy-covariance method, $Q^*$ measured, and $\Delta Q_S$ estimated using objective hysteresis model (Ferreira et al., 2013). The other SEB components (Eq. 1), such as $Q_F$ and $\Delta Q_A$ are not considered in this work. Both analyses are based on daily (24 h) and daytime ($Q^* > 0$) values evaluated from hourly and half- hourly values of the SEB components, $Q_H$, $Q_E$, $Q^*$, $\Delta Q_S$, and corresponding ratios, $\Delta Q_S/Q^*$, $Q_H/Q^*$, $Q_E/Q^*$, $Q_H/Q_E$, $Q_H/\Delta Q_S$, estimated from high-quality measurements taken at IAG site during February (summer/wet) and August (winter/dry) from 2013 to 2015, and by considering as references previous studies carried out by Ferreira et al. (2013), Oliveira et al.

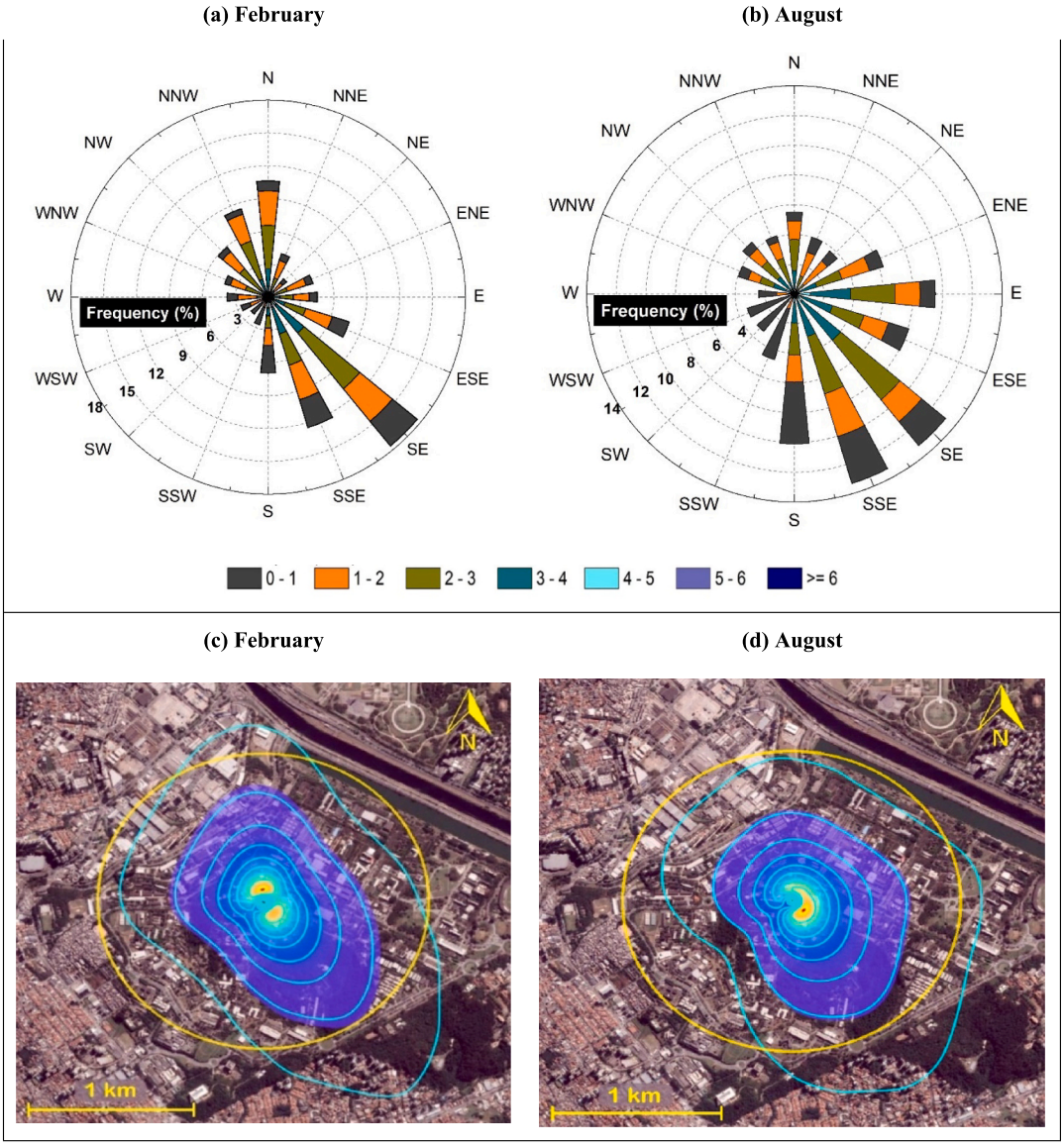


**Fig. 2.** Seasonal variation of (a)-(b) wind rose and (c)-(d) footprint in the IAG. Based on observations conducted during February and August, from 2013 to 2015. Dashed circles in (a)-(b) indicates frequency. Blue lines in (c) and (d) indicate footprint contribution varying from 90% (outer) by fixed steps of 10%. Yellow circles indicate circular areas of 1-km radius centred in the IAG. (For interpretation of the references to colour in this figure legend, the reader is referred to the web version of this article.)

(2020), and Torres et al. (2023).

*2.2.1. Net radiation, sensible and latent heat fluxes*

Net radiation measurements are conducted with a frequency of 0.2 Hz by net radiometer model CNR4 from Kipp-Zonen and recorded as 5-min averages using in a datalogger, model CR3000, manufactured by Campbell Scientific Inc. The net radiometer was set in the micrometeorological tower at 8.4 m above the platform surface.

Sensible and latent heat are obtained from turbulence measurements using a 3D sonic anemometer and gas analyser, model IRGASON, manufactured by Campbell Scientific Inc. They are estimated applying EC method in 30-min long time series of vertical wind speed, air temperature and water vapor density saw with a sampling frequency of 10 Hz. The predominant wind direction is southeast in both periods (Fig. 2a-b), therefore turbulent sensors were oriented pointing southeast to minimize the amount of contaminated data by the sensor arms and other supporting structures. Turbulent fluxes were estimated using the algorithm developed by the Laboratory of Micrometeorology of IAG (USP) named MBFlux (Mcity Brazil Flux). The MBFlux comprises the following quality control procedure to: (i) perform Webb correction, (ii) remove spikes, (iii) perform linear detrending, (iv) impose skewness and kurtosis thresholds, (v) remove non-stationary turbulent data, (vi) remove tower blocking effects and (vii) rain effects. In addition, the performance of the turbulence sensors was verified using (viii) the flags provided by the manufacturer, and by taking into consideration (ix) tilting effects caused by topography using a planar fit procedure. More details about MBFlux performance can be found in Oliveira et al. (2020) and Silveira et al. (2022).

The geometric properties, given by the turbulence measurements height of the 25.40 m and mean building heights of the 5.9 m, show that turbulence measurements carried in IAG are performed three times the mean building height, corresponding to the inertial surface layer. The systematic distortion of the flow caused building and other obstacles was also mapped using method proposed by Fortuniak et al. (2013). Details of this procedure can be found in Oliveira et al. (2020) and Silveira et al. (2022). Quality control procedures managed removing 23% of 7992 raw blocks, while the mapping of flow distortions removing 28% of the remaining blocks, totalizing in 49% of the original blocks employed.

*2.2.2. Stored energy flux*

In the urban canopy, $\Delta Q_S$ can be estimated indirectly by the objective hysteresis model (OHM) proposed by Grimmond et al. (1991). The OHM is based on the following expression:

$$\Delta Q_S = a_1\, Q^* + a_2\left(\frac{dQ^*}{dt}\right) + a_3 \tag{2}$$

Where $dQ^*/dt$ is the time rate of change for net radiation at the surface and $a_1$, $a_2$ and $a_3$ are empirical coefficients associated to response of the surface material due the energy input (Camuffo and Bernardi, 1982; Oke and Cleugh, 1987; Grimmond et al., 1991; Grimmond and Oke, 1999; Ferreira et al., 2013).

The $\Delta Q_S$ was estimated using hourly values of net radiation and average values of $a_1$, $a_2$ and $a_3$ of expression (2), based on the composition of each land use classification proposed by Grimmond and Oke (1999) (Table 2). Grimmond and Oke (1999) evaluated the OHM against the energy balance residual method as a reference in seven American cities and the results showed that the performance of the OHM was satisfactory in urban and suburban areas in conditions of weak winds ($< 2\ ms^{-1}$). According to Ferreira et al. (2013), OHM model reproduces the mean diurnal evolution of the stored energy flux in the suburban areas of São Paulo City like IAG.

*2.2.3. Anthropogenic energy flux and heat advection*

Anthropogenic energy flux in the IAG region is not considered in this work because the energy released by vehicular, stationary, and metabolic sources in this site are smaller than the average value for the city of São Paulo (20 $Wm^{-2}$) proposed by Ferreira et al. (2011). Indeed, Ribeiro et al. (2018) showed that the intensity of UHI in São Paulo is more realistically simulated by the WRF-model by assuming $Q_F$ equal to 11.2 $Wm^{-2}$ for low density residential fraction, a land use class like one at the IAG (Section 2.1.4).

Similarly, $\Delta Q_A$ is not considered here because advection term cannot be estimated using only SEB measurements in one-point site with heterogeneous land use as IAG. As mentioned before, quantifying the impact of the horizontal heat advection on SEB is problematic in urban areas due to difficulties in to estimate the site position relative to the regional flow direction and contrasting surfaces

**Table 2**
Land use fraction (LUF) in the area within 1-km radius circle centred at the IAG. Empirical coefficients (**$a_1$, $a_2$ and $a_3$**) used in OHM are based on Grimmond and Oke (1999).

| Surface type | Land use fraction | Coefficients | | | OHM Parameters | | |
|---|---|---|---|---|---|---|---|
| | LUF | $a_1$ | $a_2$ ($h^{-1}$) | $a_3$ ($W\ m^{-2}$) | LUF×$a_1$ | LUF×$a_2$ ($h^{-1}$) | LUF×$a_3$ ($W\ m^{-2}$) |
| Greenspace/open | 0.359 | 0.34 | 0.41 | −35.00 | 0.12 | 0.15 | −12.57 |
| Paved/impervious | 0.450 | 0.78 | 0.45 | −43.00 | 0.35 | 0.20 | −19.35 |
| Rooftop[1] | 0.151 | 0.26 | 0.91 | −23.00 | 0.04 | 0.14 | −3.47 |
| Canyon | 0.040 | 0.52 | 0.03 | −34.00 | 0.02 | 0.00 | −1.36 |
| **Total** | **1.000** | | | | **0.53** | **0.49** | **−36.75** |

[1] Rooftop coefficients employed in the OHM by Meyn and Oke (2009).

(Grimmond and Oke, 1995; Foken, 2008; Cuxart et al., 2016; Båserud et al., 2020; Mauder et al., 2020).

### 2.2.4. Closure parameters

The energy balance closure (EBC) parameter (Eq. (3)) is based on the 1st thermodynamic law and usually accepted as a standard procedure to evaluate the SEB closure in surface-atmosphere exchange studies (Wilson et al., 2002; Oliphant et al., 2004; Moriwaki and Kanda, 2004).

$$EBC = (Q^* - \Delta Q_S) - (Q_H + Q_E) \quad (3)$$

EBC parameter is evaluated using two different methods: Simple Linear Regression (SLR) and energy balance ratio (EBR). The SLR method is based on a simple linear regression analysis by fitting a straight line through the point cloud in a scatter plot of ($Q^*$ - $\Delta Q_S$) against ($Q_H + Q_E$) (Eq. (4)). The second method was proposed by Wilson et al. (2002) and is based on the Energy Balance Ratio (EBR, Eq. (5)) between the sum of ($Q^*$- $\Delta Q_S$) and ($Q_H + Q_E$) over specified time periods.

$$(Q_H + Q_E) = \beta_0 + \beta_1 (Q^* - \Delta Q_S) \quad (4)$$

$$EBR = \frac{\sum (Q_H + Q_E)}{\sum (Q^* - \Delta Q_S)} \quad (5)$$

### 2.2.5. Footprint

Footprint analyses are needed for understanding flux tower measurements in heterogenous areas (Leclerc and Foken, 2014). Despite all limitations, footprint models yield an objective estimate of both, position and size of surface source areas, and their relative contribution to the measured fluxes. It is especially important for upscaling from single point flux measurements to local or regional scale (Kormann and Meixner, 2001; Neftel et al., 2008; Kljun et al., 2015). In this work the footprint of flux measurements conducted in the IAG (Fig. 2) is evaluated using Flux Footprint Prediction (FFP) model developed by Kljun et al. (2015). FFP model uses as input 30-min values of wind speed and direction, cross wind standard deviation, friction velocity, Obukhov length and UBL height. These variables are estimated from measurements conducted during February and August, from 2013 to 2015, and using MBFLux (Oliveira et al., 2020). During night-time UBL height is estimated using 30-min values of friction velocity and Obukhov length in empirical expression (Oliveira et al., 2020). During daytime UBL height is set constant and equal to 1500 m (Silveira et al., 2022).

## 3. Seasonal variation of SEB

Seasonal variation of the SEB components is analysed by considering the diurnal cycles of monthly average hourly values of $Q^*$, $Q_H$, $Q_E$ and $\Delta Q_S$ during February and August, assumed here as typical summer/wet and winter/dry months in São Paulo City (Fig. 3). Similarly, major features of the SEB components and corresponding ratios ($\Delta Q_S/Q^*$, $Q_H/Q^*$, $Q_E/Q^*$, $Q_H/Q_E$, $Q_H/\Delta Q_S$) are also analysed in this section by considering monthly average daily (24 h) and daytime ($Q^* > 0$) values corresponding to the time integral over

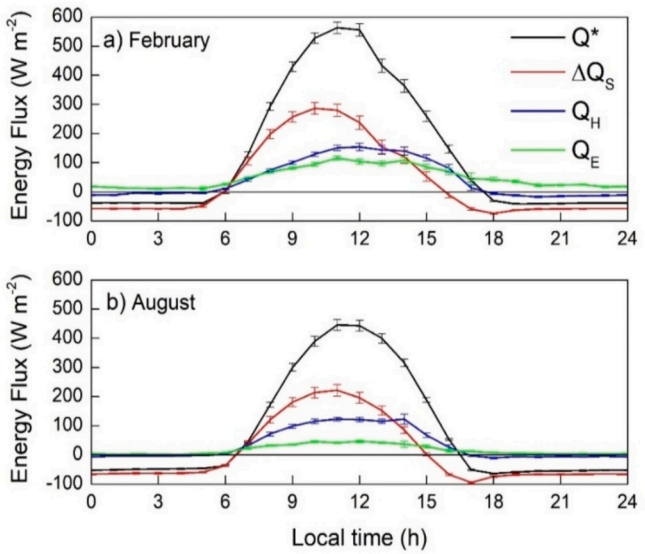


**Fig. 3.** Seasonal variation of the diurnal evolution of the monthly average hourly values of the observed ($Q^*$, $Q_H$ and $Q_E$) and simulated ($\Delta Q_S$) SEB components in the IAG during February (summer/wet season) and August (Winter/dry season). Vertical bars correspond to the statistical error of the mean.

24-h period and during period when Q* > 0 respectively (Table 3). These last parameters allow an objective comparison between the daily and daytime values estimated in this study and those previously estimated in São Paulo and in other urban and suburban areas located in middle and subtropical latitudes (Oke, 1988; Grimmond, 1992; Grimmond and Oke, 1999; Moriwaki and Kanda, 2004; Balogun et al., 2009; Goldbach and Kuttler, 2013).

February (rainy season) and August (dry season) can be used as reference months to characterize the climatic conditions during summer and winter in the city of São Paulo due to the greater contrast in terms of precipitation. Therefore, the seasonal variation can be detected by comparing monthly average daily and hourly values of the SEB main components observed during February and August if the mean meteorological conditions during the observational time span do not differ significantly from the normal conditions. As indicated in Supplementary Table S3, the meteorological conditions at IAG do not diverge from the climate conditions in the MRSP (Section 2.1.1). Differences observed during 2013–15 are related to spatial variability of moisture and temperature caused by the proximity of the Atlantic Ocean, land use and topographic effects.

### 3.1. Footprint

To examine the contribution of all source areas to the turbulent fluxes estimated at IAG site is necessary to examine the wind rose, based on wind measurements performed at IAG site simultaneously to the periods of time when turbulent fluxes estimates are considered valid by the quality control procedures of MBFlux, showing which wind sectors are most frequently observed in the flux site (Fig. 2a-b). The average land use composition that influenced turbulent exchanges, was divided in 8 sectors according to the individual frequency of 30-min mean wind speed and direction measured at the IAG (Fig. 1d).

The predominant wind directions in the IAG indicates that vegetated area located at *SE*-S sector and within 1-km radius circle area remains aligned upwind most of the time, may impact the turbulent fluxes measured at IAG. The SE-S sector is arranged by 8% of midrise building roof (LCZ 5 mainly), 24% of impervious surface (parking and street) and 66% of woodland and 2% of vegetation. The E-SE sector is arranged by 16% of low-rise and midrise building roof (LCZ 5 and LCZ 6), 30% of impervious surface (parking and street) and 53% of woodland and 1% of vegetation detailed in Supplementary Table S4.

In February, at IAG the wind directions are from SE-S sector in 37% of the time, and from NW-N sector in 25% (Fig. 2a). In August, wind directions are from SE-S sector in 37%, and from E-SE sector in 31% of the time (Fig. 2b). In February, the strongest winds are from 135° and 157.5°, with wind speed larger than 2 m $s^{-1}$ in 15% and 10% of the time. In August, the strongest winds are from 135° and 157.5°, observed in respectively 11% and 10% of the time.

In February, the main source areas that contribute to the turbulent fluxes measured at IAG site are indicated by bluesish area inside of the 80% isopleth (Fig. 2c), that elongates toward the prevailing wind direction from SE-S sector and characterized by a strong presence from woodland and vegetation (Atlantic Forest reserve). A secondary source area is shown by 80%-isopleth elongation in wind direction from NW-N and originated from parking, street, and building roofs (Fig. 2c). In August, the main source area of turbulent fluxes includes extensive green area (woodland and vegetation) in the prevailing wind direction SE-S and E-SE sectors (Fig. 2d).

As reported by Masseroni et al. (2014), the effects of the scale factor due to the heterogeneity of the radiation and turbulence sensor footprint can affect the energy balance closure by up to 9.7 $Wm^{-2}$ when analysing the footprint of the source area for each energy balance flux. Atmospheric stability conditions, sensor height, surface roughness, and wind speed are common parameters governing footprint models. Specific local experiments are needed to understand how the contribution area of turbulent fluxes changes based on the atmospheric, physical, and geometric characteristics of the surface.

**Table 3**
Seasonal variation of SEB components and ratios in the IAG. Monthly average daily (24 h) and daytime (Q* > 0) values observed during February and August between 2013 and 2015. Typical ranges correspond to suburban areas in mid-latitudes cities.

| daily value | | | | | | | | | |
|---|---|---|---|---|---|---|---|---|---|
| Month (Season) | SEB components (MJ $m^{-2}$ $d^{-1}$) | | | | SEB-components ratio | | | | |
| | Q* | $\Delta Q_S$ | $Q_H$ | $Q_E$ | $\Delta Q_S$ / Q* | $Q_H$ / Q* | $Q_E$ / Q* | $Q_H$ / $Q_E$ | $Q_H$ / $\Delta Q_S$ |
| February (Summer/ Wet) | 11.82 ± 0.70 | 3.31 ± 0.75 | 3.75 ± 0.62 | 4.28 ± 0.36 | 0.28 ± 0.06 | 0.32 ± 0.09 | 0.36 ± 0.18 | 0.88 ± 0.07 | 1.13 ± 0.16 |
| August (Winter/Dry) | 7.31 ± 0.57 | 0.82 ± 0.28 | 2.99 ± 0.26 | 1.51 ± 0.19 | 0.11 ± 0.05 | 0.41 ± 0.08 | 0.21 ± 0.06 | 1.98 ± 0.13 | 3.65 ± 0.09 |
| [a]Typical Range | 2.89 to 15.58 | −1.09 to 5.86 | 1.99 to 7.73 | 0.93 to 6.80 | −0.12 to 0.61 | 0.23 to 0.82 | 0.12 to 0.46 | 1.11 to 4.16 | −61.95 to 15.15 |
| daytime value (Q* > 0) | | | | | | | | | |
| February (Summer/ Wet) | 13.39 ± 0.75 | 5.95 ± 0.51 | 4.11 ± 0.69 | 3.27 ± 0.57 | 0.44 ± 0.05 | 0.31 ± 0.09 | 0.24 ± 0.05 | 1.26 ± 0.10 | 0.69 ± 0.15 |
| August (Winter/Dry) | 9.74 ± 0.57 | 4.17 ± 0.58 | 3.12 ± 0.26 | 1.18 ± 0.19 | 0.43 ± 0.09 | 0.32 ± 0.19 | 0.12 ± 0.04 | 2.64 ± 0.20 | 0.75 ± 0.11 |
| [b]Typical Range | 6.67 to 17.49 | 2.01 to 5.45 | 2.20 to 8.49 | 0.70 to 6.24 | 0.17 to 0.65 | 0.20 to 0.62 | 0.07 to 0.37 | 1.24 to 2.87 | 0.64 to 3.73 |

[a,b] Grimmond and Oke, 1999, [a,b] Moriwaki and Kanda, 2004; [a,b] Balogun et al., 2009; [a,b] Goldbach and Kuttler, 2013.

### 3.2. Net radiation

The diurnal cycle of Q* is determined mostly by the incoming shortwave radiation during daytime and outgoing longwave radiation during night-time. The amplitude of Q* is larger in February during daytime and in August during night-time (Fig. 3). This pattern can be explained by a combination of astronomical factors and the seasonal variation of the atmospheric moisture content (Ferreira et al., 2012; Oliveira et al., 2020). During August (winter/dry season) night-time longwave emission from surface is larger compared to February (summer/wet season).

### 3.3. Stored energy flux

Daytime $\Delta Q_S$ maximum occurs before Q* in February and at the same time (in phase) in August (Fig. 3). Similarly, during both months $\Delta Q_S$ and Q* reach minimum before sunset, and $\Delta Q_S$ becomes negative before of Q*. They recover and remain practically constant up to sunrise. The energy lost by the surface during night-time ($Q^* < 0$) is almost totally offset by $\Delta Q_S$ release in the suburban canopy.

### 3.4. Sensible and latent heat

As expected, the seasonal variation of $Q_H$ and $Q_E$ diurnal cycles in the suburban area of São Paulo Megacity, with land use characteristics like the IAG site, depend mostly on seasonal changes in vegetation and soil moisture content (Ferreira et al., 2013). In February (summer/wet season), the peak in $Q_H$ occurs one hour after Q* (Fig. 3a). In August (winter/dry season), daytime maximum in $Q_H$ and Q* occur at the same time (Fig. 3b). In both seasons, $Q_H$ becomes negative after sunset, at same time as Q*, staying negative (and small) until sunrise, while $Q_E$ remains positive and small (but magnitude larger then $Q_H$).

Thus, more water and solar radiation are available in the summer/wet season, so that a well-developed vegetation is performing more photosynthesis, and more evapotranspiration is observed. Therefore, the diurnal cycle of $Q_H$ is delayed in relation to Q*, due to higher $Q_E$ (evapotranspiration). In the winter/dry season, less water and solar radiation reduce evapotranspiration so that $Q_H$ is in phase with Q*, and diurnal cycle of SEB in the suburban area of São Paulo has urban behaviour (Goldbach and Kuttler, 2013).

### 3.5. SEB component ratios

The impact of urbanization is to favour partitioning of energy available in the surface into sensible rather than latent heat and to increase heat storage by the urban canopy. The suburban and urban surfaces are characterized by rather variable energy partitioning, largely controlled by moisture availability. When both the urban and rural areas are wet, differences between the energy turbulent fluxes are small; in drier conditions the city tends to become a regional source of sensible heat, although increasing water availability can mitigate this tendency (Oke, 1982).

#### 3.5.1. Net radiation ratios

In August, monthly average daily and daytime values of net radiation ratios ($\Delta Q_S$ / Q*, $Q_H$ / Q*, $Q_E$ / Q*) in the IAG site are outside of the expected range for suburban areas (Table 3). A possible explanation for this discrepancy may be related to the large fraction of impervious land use in the IAG (Table 4), that favours the storage of heat in the substrate detrimental to $Q_H$ and $Q_E$. The other ratios are like the ones obtained by Ferreira et al. (2013) and Oliveira et al. (2020). This shows that partition of Q* among $\Delta Q_S$, $Q_H$ and $Q_E$ in the IAG are consistent with expected for suburban areas.

#### 3.5.2. Bowen ratio

Bowen ratio, estimated from monthly average daily values of $Q_H$ and $Q_E$, varies from 0.88 (February) to 1.98 (August) in the IAG

**Table 4**
Land use fraction in the circular area of 1-km radius centred and Bowen ratio in the IAG. Others suburban and urban areas of nine (eight mid-latitude and one subtropical) cities are based on Grimmond and Oke (1999) and Moriwaki and Kanda (2004).

| Location | Season | Green space | Paved / impervious | Rooftop | Canyon | Bowen ratio | |
|---|---|---|---|---|---|---|---|
| | | | | | | Daily (24 h) | Daytime ($Q^* > 0$) |
| Kugahara, Tokyo | Summer | 0.21 | 0.38 | 0.33 | 0.03 | 2.37 | 2.85 |
| Chicago, IL | | 0.24 | 0.14 | 0.23 | 0.38 | 1.11 | 1.24 |
| Miami, FL | Spring | 0.26 | 0.24 | 0.29 | 0.21 | 1.47 | 1.55 |
| Tucson, AZ | Summer | 0.28 | 0.33 | 0.19 | 0.20 | 1.58 | 2.08 |
| San Gabriel, LA | | 0.31 | 0.26 | 0.26 | 0.14 | 2.13 | 2.17 |
| Vancouver, BC | Summer-Autumn | 0.33 | 0.17 | 0.22 | 0.29 | 2.72 | 2.87 |
| São Paulo City, SP | Summer/wet (Feb) | 0.36 | 0.45 | 0.15 | 0.04 | 0.88 | 1.26 |
| | Winter/dry (Aug) | | | | | 1.98 | 2.64 |
| Sacramento, CA | Summer | 0.42 | 0.10 | 0.30 | 0.15 | 1.14 | 1.26 |
| Arcadia, LA, CA | | 0.47 | 0.17 | 0.22 | 0.12 | 1.60 | 1.61 |
| Arcadia, LA, CA | | 0.49 | 0.16 | 0.21 | 0.12 | 1.21 | 1.24 |

(Table 3). These values, based on three years of observation (2013-2015), agree very well with 0.90 (February) and 2.12 (August), saw during 10 days in February (19–28) and August (6–15) of 2013 by Oliveira et al. (2020) in the IAG site. On the other hand, monthly average daytime values of $Q_H$ and $Q_E$ yielded larger Bowen ratios in the IAG, varying from 1.26 (February) to 2.64 (August). These values, based on three years of observation (2013-2015), do not also differ significantly from the ones estimated from 10-days average daily and daytime values by Oliveira et al. (2020) during February and August of 2013 in the IAG site. Furthermore, during both months Bowen ratios in the IAG display values within the range seen in suburban areas of mid and subtropical latitudes cities (Table 4).

On the other hand, Bowen ratio based on monthly average daytime values, vary from 1.26 in February to 2.64 in August. The Bowen ratio increased from 0.88 to 1.98 with decreasing soil moisture at the IAG, and the monthly average $Q_E$ daily values decreased from 4.28 MJ $m^{-2}$ $d^{-1}$ in February (wet season) to only 1.51 MJ $m^{-2}$ $d^{-1}$ in August (dry season). Equivalent reduction is seen in the case of the daytime values. During summer/wet season, the Bowen ratio saw in the IAG are within the range saw in suburban areas of midlatitudes cities. During winter/dry season, Bowen ration in the suburban area of São Paulo agree with upper limits of the range observed in midlatitude cities (Table 4).

### *3.5.3. Stored energy fraction (QH / ΔQS)*

In February there is more energy available to be stored in the canopy as $\Delta Q_S$ and transferred to the atmosphere as $Q_H$ and $Q_E$. During daytime, a large fraction of the net radiation available at the surface is transferred to the urban canopy by conduction ($\Delta Q_S > 0$), a small fraction goes to the atmosphere by turbulent convection ($Q_H > 0$), and even smaller by evapotranspiration at the surface ($Q_E > 0$) (Fig. 3). Ratios of sensible heat flux to the stored energy flux in both months and Bowen ratio in February in the IAG show values outside of the expected interval values for suburban areas.

## 4. SEB closure

The EBC estimated from SLR method is showed in Fig. 4. The results are based in the relationship between half-hourly values of input ($Q^*$- $\Delta Q_S$) and output ($Q_H + Q_E$) of energy fluxes observed in February and August from 2013 to 2015 in the IAG. The straight line obtained by SLR can be expressed as $(Q_H + Q_E) = 10.72 + 0.79$ ($Q^*$ - $\Delta Q_S$) for February and as $(Q_H + Q_E) = 1.13 + 0.75$ ($Q^*$ - $\Delta Q_S$) for August. They correspond to output of energy flux equal to 21% and 25% smaller than the input of energy flux, respectively.

Considering only daytime half-hourly values ($Q^* > 0$) (not shown in Fig. 4) the SRL method the resulting straight lines are $(Q_H + Q_E) = 50.02 + 0.64$ ($Q^*$ - $\Delta Q_S$) and $(Q_H + Q_E) = 41.10 + 0.55$ ($Q^*$ - $\Delta Q_S$) for February and August, respectively. These results indicate an output of energy flux 36% and 45% smaller than the input of energy flux respectively, indicating that SEB in the suburban region of São Paulo (Table 5) indicate that the available energy is in the upper half of the 50-site range reported by Wilson et al. (2002).

Table 5 show that the $\beta_0$ (Y-axis intercepts range) of the linear regression fitted curve for February and August (Fig. 4) agreed with Wilson et al. (2002). In general, the daily and daytime half-hourly values of the output energy ($Q_H + Q_E$) and input energy ($Q^*$- $\Delta Q_S$) shows RMSE and $R^2$ values in February and August presents values with good agreement between the input and output of energy ratio ($\beta_I$) in the urban canopy. The determination coefficient ($R^2$) agrees with all sites used in the analysis by Wilson et al. (2002) and Oliphant et al. (2004).

The non-closure of energy balance in São Paulo City during daily (21% in February and 25% in August) and daytime (36% in February and 45% in August) periods the same order of magnitude observed in other studies described in Wilson et al. (2002) and Oliphant et al. (2004).

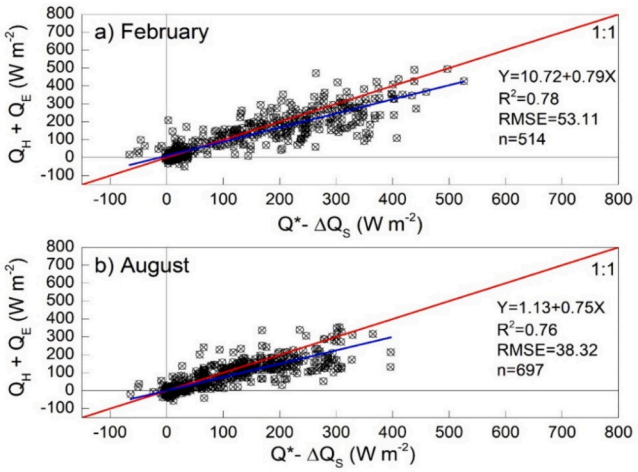


**Fig. 4.** Dispersion diagram of half-hourly values of output ($Q_H + Q_E$) versus input ($Q^*$ - $\Delta Q_S$) of the EBC in a) February and b) August. Linear regression lines of the best fit are indicated by blue. Correlation coefficients are shown by $R^2$, root mean square error by RMSE, and n is the number of values. (For interpretation of the references to colour in this figure legend, the reader is referred to the web version of this article.)

**Table 5**
Linear regression coefficients of the SLR method, statistical parameters based on half-hourly values of EBC components in February and August for three years (2013 to 2015).

| | Daily | | | | Daytime | | | |
|---|---|---|---|---|---|---|---|---|
| Parameter | February | August | #Range | #Mean | February | August | #Range | #Mean |
| $\beta_0$ (Y-axis Intercept in $Wm^{-2}$) | 10.72 | 1.13 | −32.9 to 36.9 | 3.70 | 50.02 | 41.10 | No available | −0.3 |
| $\beta_1$ (Slope) | 0.79 | 0.75 | 0.53 to 0.99 | 0.79 | 0.64 | 0.55 | 0.56 to 0.97 | 0.80 |
| RMSE ($Wm^{-2}$) | 53.11 | 38.32 | No available | | 66.74 | 50.51 | No available | |
| $R^2$ | 0.78 | 0.76 | 0.64 to 0.96 | 0.86 | 0.54 | 0.44 | No available | 0.81 |
| n | 514 | 697 | 2954 to 15,638 | 8607 | 281 | 621 | No available | |
| EBC (MJ $m^{-2}$ $d^{-1}$) | 1.33 | 1.57 | No available | | 2.16 | 2.46 | No available | |

# Source: Wilson et al. (2002) and Oliphant et al. (2004).

The EBC estimated from EBR method (Fig. 5) shows diurnal evolution of monthly average hourly values of EBC, EBR, ($Q_H + Q_E$) and ($Q^* - \Delta Q_S$) during February and August in the IAG. Table 6 display monthly average daily (24 h) and daytime ($Q^* > 0$) values of EBC and EBR displayed in Fig. 5.

The monthly average hourly values of EBR during the daily period was 0.70 in February (wet season) and 0.69 in August (dry season) and daytime values was 0.86 in February and 0.72 in August (Table 6). According to Wilson et al. (2002) the ratio of mean values of daily and daytime turbulent heat flux of available energy for 50 sites analysed was 0.84 and 0.80, respectively. Between morning and evening transition periods, when the mean values of ($Q^* - \Delta Q_S$) is close to zero, the EBR is not significant. During transition periods, when $Q^* > 0$, the EBR remained practically constant in February and decrease from the morning to afternoon during August.

The results are based in the cumulatively sum of the ($Q^* - \Delta Q_S$) and ($Q_H + Q_E$) over specified time periods, calculated through the ratio between the output and input of energy. The daily value of output is equal to 30% and 31% smaller than the input of energy flux. In contrast the values correspond to output of energy flux are equal to 14% and 28% smaller than the input of energy flux during daytime period. These estimates of EBC showed in the Table 6 show that the available energy in February and August presents values with good agreement between the input and output of energy ratio in the suburban canopy the according to Wilson et al. (2002).

## 5. Conclusion

Hourly and half-hourly values of $Q^*$, $Q_H$, $Q_E$, $\Delta Q_S$ were estimated for the IAG site, in a suburban area in the City of São Paulo, using high-quality observations and OHM model during February (summer/wet) and August (winter/dry) between 2013 and 2015. All measurements used in this study were performed in a 10-m tower at the top of a 4-story building of the Institute of Astronomy, Geophysics, and Atmospheric Sciences, in the University of São Paulo campus, a suburban area west São Paulo City. The IAG site belongs to the observational network of three micrometeorological towers of the MCITY BRAZIL Project (Oliveira et al., 2020, Sánchez et al., 2020, Silveira et al., 2022, Sánchez et al., 2022, Moreira et al., 2022a-b, Torres et al., 2023), that has been expanded to four by the BIOMASP+ Project.

The analysis of SEB components in the IAG site shows that:

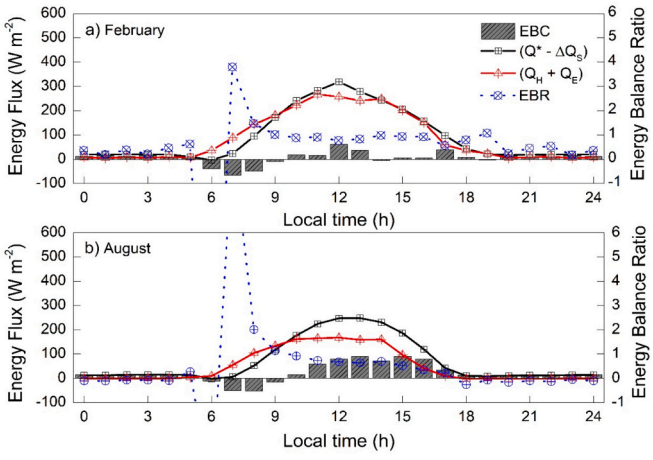


**Fig. 5.** The monthly average hourly values of energy balance closure (EBC), energy balance ratio (EBR), energy flux input ($Q^* - \Delta Q_S$) and energy flux output ($Q_H + Q_E$) observed in February and August from 2013 to 2015 in the IAG.

**Table 6**
Summary of energy balance closure (EBC) and EBR method in the IAG. Daily (24 h) and daytime (Q* > 0) values for February and August from 2013 to 2015.

| | EBC (MJ $m^{-2}$ $d^{-1}$) | | EBR | | | |
|---|---|---|---|---|---|---|
| | February | August | February | August | [$]Range | [$]Mean |
| **Daily** | 0.50 | 1.96 | 0.70 | 0.69 | 0.34–1.69 | 0.84 |
| **Daytime** | 0.28 | 0.99 | 0.86 | 0.72 | No available | 0.80 |

[$] Source: Wilson et al. (2002).

- In this suburban environment, the sensible energy flux (conduction and advection) is the major source of energy during daytime, due mainly to the substantial amounts of energy stored in the urban fraction of suburban canopy during daytime.
- The daily values of evapotranspiration are relatively important remaining positive during both summer/dry and winter/dry season months, represented by February and August, respectively, due presence of extensive greenspace located at SE-S sector, a predominant wind direction in both months. Sector SE-S formed by 66% of woodland and 2% of vegetation.
- During the day in both seasons, the stored energy flux is the mirror image of the sensible energy flux, shared between conduction and convection as reported in Ferreira et al. (2013) for May.

In February and August, the diurnal cycles of sensible heat ($Q_H$) and latent heat ($Q_E$) appear to respond to the extent of vegetation and tree cover in the S-SE sector, as showed by the footprint model. This suggests that the source area of the observed fluxes agrees on a local scale in February. The diurnal values of $Q_H$ are predominant and respond well to the extent of impermeable surface cover (NW-N sector) estimated by the footprint model. In August, both daily and diurnal values of sensible heat flux are predominant and respond well to the extent of impermeable surface cover estimated by the footprint model, confirmed by the decrease in moisture supply for evapotranspiration during the dry season.

The results show that physical processes, such as radiation reflection and absorption, affect the distribution of received energy depending on surface properties, showing the relative dominance of observed sensible or latent heat fluxes in February and August. When examining the energy balance closure residual, where we assess $Q_H$, $Q_E$, and $\Delta Q_S$ in relation to total net radiation over observations and parameterizations conducted over three years in February and August, we can conclude that the largest gap observed in closure occurred in August, with 25% for daily values and 45% for daytime values, respectively. This is more likely caused by underestimated the heat stored in the soil and canopy layer.

Furthermore, it is necessary to highlight that the seasonal variation of the diurnal cycle of the SEB main components is disrupted by circulation patterns in the city of São Paulo. During the night and morning, surface winds are predominantly from the NW-N sector, associated with the semi-stationary South Atlantic Subtropical High-Pressure System. In the afternoon and early evening, this large-scale pattern changes significantly by the sea breeze intrusions into the city on >50% of days, increasing the intensity of surface wind, altering its direction to the SE, and bringing moister and cooler air from the Atlantic Ocean.

The daily (24 h) and daytime ($Q^* > 0$) values of energy fluxes based on the SRL and EBR methods during February (summer/wet) and August (winter/dry) showed a good agreement between the input and output of energy in the urban canopy. The output energy ($Q_H + Q_E$) and input energy ($Q^* - \Delta Q_S$) based on both methods presented a good agreement with RMSE and $R^2$. However, errors associated with factors (instrument error, data processing error, other sources of energy and sub-mesoscale transport, secondary circulations) that affect the flux estimates described here need to be addressed, so the contribution of anthropogenic heat and horizontal advection of energy fluxes.

The non-closure of the SEB documented in this study may have occurred due to factors and processes described in the introduction (Table 1). The SEB is influenced by a wide range of physical, chemical, and biological processes occurring in the atmospheric boundary layer. When some of these processes are not adequately quantified in observations, they can compromise the EBC (Mauder et al., 2020). In the case of the suburban area of São Paulo city, seasonality, variations in land cover, and changes in vegetation composition were considered in closing the energy balance. However, errors associated with other sources of energy (anthropogenic heat and horizontal advection of energy), sub-mesoscale transport, and secondary circulations that may affect flux estimates, were not evaluated due to technical limitations in single-tower observations.

The research has yielded results that highlight the importance of estimating the components of the Surface Energy Balance (SEB) and conducting the Energy Balance Closure (EBC) to better assess induced changes in climate patterns and energy distribution in the study area. The SEB and EBC have contributed to a deeper understanding of energy exchanges in the surface-canopy-atmosphere system in a suburban area of high-altitude subtropical climate (Cwb), offering consistent insights to aid in the development of more accurate meteorological and hydrological models, essential for urban planning. For instance, it serves as a starting point for using the knowledge from SEB and EBC to analyse the technical feasibility of implementing Low Impact Development (LID) practices, based on the concept of preserving and restoring natural resources (Ferreira and da Rocha, 2023).

## CRediT authorship contribution statement

**Mauricio Jonas Ferreira:** Writing – review & editing, Writing – original draft, Visualization, Validation, Methodology, Investigation, Formal analysis, Data curation, Conceptualization. **Amauri Pereira de Oliveira:** Writing – review & editing, Writing – original draft, Visualization, Validation, Supervision, Software, Resources, Project administration, Methodology, Investigation, Funding

acquisition, Formal analysis, Data curation, Conceptualization. **Lucas Cardoso da Silveira:** Visualization, Validation, Formal analysis, Data curation, Conceptualization. **Georgia Codato:** Visualization, Validation, Data curation, Conceptualization. **Adalgiza Fornaro:** Visualization, Validation, Formal analysis, Data curation, Conceptualization. **Agnès Borbon:** Visualization, Validation, Formal analysis, Data curation, Conceptualization.

## Declaration of competing interest

The authors declare that they have no known competing financial interests or personal relationships that could have appeared to influence the work reported in this paper.

## Data availability

Data will be made available on request.

## Acknowledgments

This research was sponsored by the Brazilian Research Foundations: FAPESP (2011/50178-5; 2020/07141-2; 2022/02616-8), FAPERJ (E26/111.620/2011; E26/103.407/2012), CNPq (476812/2011-9; 462734/2014-5; 304786/2018-7) and CAPES (CAPES 001). This work was also sponsored by the Slovenian Research Agency (LI-4154A, L2-5457C, L2-6762C).

## Appendix A. Supplementary data

Supplementary data to this article can be found online at https://doi.org/10.1016/j.uclim.2024.102008.

## References

Aubinet, M., Grelle, A., Ibrom, A., Rannik, Ü., Moncrieff, J., Foken, T., Kowalski, A.S., Martin, P.H., Berbigier, P., Bernhofer, Ch., Clement, R., Elbers, J., Granier, A., Grünwald, T., Morgenstern, K., Pilegaard, K., Rebmann, C., Snijders, W., Valentini, R., Vesala, T., 2000. Estimates of the annual net carbon and water exchange of European forests: the EUROFLUX methodology. Adv. Ecol. Res. 30, 114–175. https://doi.org/10.1016/S0065-2504(08)60018-5.

Balogun, A.A., Adegoke, J.O., Vezhapparambu, S., Mauder, M., McFadden, J.P., Gallo, K., 2009. Surface energy balance measurements above an exurban residential neighbourhood of Kansas City, Missouri. Bound.-Layer Meteorol. 133 (3), 299–321. https://doi.org/10.1007/s10546-009-9421-3.

Båserud, L., Reuder, J., Jonassen, M., Bonin, T., Chilson, P., Jiménez, M., Durand, P., 2020. Potential and limitations in estimating sensible-heat-flux profiles from consecutive temperature profiles using remotely piloted aircraft systems. Bound.-Layer Meteorol. 174, 145–177. https://doi.org/10.1007/s10546-019-00478-9.

Bechtel, B., Daneke, C., 2012. Classification of local climate zones based on multiple earth observation data. IEEE J. Sel. Top. Appl. Earth Obs. Remote Sens. 5 (4), 1191–1202. https://doi.org/10.1109/JSTARS.2012.2189873.

Bechtel, B., Alexander, P.J., Böhner, J., Ching, J., Conrad, O., Feddema, J., Mills, G., See, L., Stewart, I., 2015. Mapping local climate zones for a worldwide database of the form and function of cities. ISPRS Int. J. Geo Inf. 4, 199–219. https://doi.org/10.3390/ijgi4010199.

Bechtel, B., Alexander, P.J., Beck, C., Böhner, J., Brousse, O., Ching, J., Demuzere, M., Fonte, C., Gál, T., Hidalgo, J., 2019. Generating WUDAPT level 0 data–current status of production and evaluation. Urban Clim. 27, 24–45. https://doi.org/10.1016/j.uclim.2018.10.001.

Berg, A., Lintner, B.R., Findell, K.L., Malyshev, S., Loikith, P.C., Gentine, P., 2014. Impact of soil moisture–atmosphere interactions on surface temperature distribution. J. Clim. 27 (21), 7976–7993. https://doi.org/10.1175/JCLI-D-13-00591.1.

Camuffo, D., Bernardi, A., 1982. An observational study of heat fluxes and the relationship with net radiation. Bound.-Layer Meteorol. 23, 359–368. https://doi.org/10.1007/BF00121121.

Chen, Y., Jiang, W.M., Zhang, N., He, X.F., Zhou, R.W., 2009. Numerical simulation of the anthropogenic heat effect on urban boundary layer structure. Theor. Appl. Climatol. 97 (1–2), 123–134. https://doi.org/10.1007/s00704-008-0054-0.

Christen, A., Vogt, R., 2004. Energy and radiation balance of a central European City. Int. J. Climatol. 24 (11), 1395–1421. https://doi.org/10.1002/joc.1074.

Coutts, A., Beringer, J., Tapper, N., 2010. Changing urban climate and $CO_2$ emissions: implications for the development of policies for sustainable cities. Urban Policy Res. 28 (1), 27–47. https://doi.org/10.1080/08111140903437716.

Cui, W., Chui, T.F.M., 2021. Measurements and simulations of energy fluxes over a high-rise and compact urban area in Hong Kong. Sci. Total Environ. 765, 142718 https://doi.org/10.1016/j.scitotenv.2020.142718.

Cuxart, J., Wrenger, B., Martinez-Villagrasa, D., Reuder, J., et al., 2016. Estimation of the advection effects induced by surface heterogeneities in the surface energy budget. Atmos. Chem. Phys. 16 (14), 9489–9504. https://doi.org/10.5194/acp-16-9489-2016.

Droste, A.M., Steeneveld, G.J., Holtslag, A.A.M., 2018. Introducing the urban Wind Island effect. Environ. Res. Lett. 13 (9), 094007 https://doi.org/10.1088/1748-9326/aad8ef.

Duarte, D.H.S., Shinzato, P., Gusson, C.S., Alves, C.A., 2015. The impact of vegetation on urban microclimate to counterbalance built density in a subtropical changing climate. Urban Clim. 14 (December), 224–239. https://doi.org/10.1016/j.uclim.2015.09.006.

Eder, F., De Roo, F., Kohnert, K., et al., 2014. Evaluation of two energy balance closure parametrizations. Bound.-Layer Meteorol. 151, 195–219. https://doi.org/10.1007/s10546-013-9904-0.

EPC, 2020a. Environmental Planning Coordination. Available at. https://www.infraestruturameioambiente.sp.gov.br/cpla/mapa-de-cobertura-da-terra-do-estado-de-sao-paulo/ (Accessed 22 Sep 2022).

EPC, 2020b. Environmental Planning Coordinator. Homogeneous Units for the Use and Occupation of Urban Soil in the São Paulo State. Secretary for Infrastructure and Environment of the São Paulo State, São Paulo, SP, Brazil. Available at. http://s.ambiente.sp.gov.br/cpla/Ficha_Tecnica_UHCT.pdf (Accessed 22 Sep 2022).

Fallmann, J., Forkel, R., Emeis, S., 2016. Secondary effects of urban heat island mitigation measures on air quality. Atmos. Environ. 125 (Part A), 199–211. https://doi.org/10.1016/j.atmosenv.2015.10.094.

Fang, C., Wang, S., Li, G., 2015. Changing urban forms and carbon dioxide emissions in China: a case study of 30 provincial capital cities. Appl. Energy 158, 519–531. https://doi.org/10.1016/j.apenergy.2015.08.095.

Ferreira, M.J., da Rocha, H.R., 2023. Green roof infrastructure outperforms grey technology in flood mitigation in São Paulo's urbanized region. Front. Built. Environ. 9, 1254942. https://doi.org/10.3389/fbuil.2023.1254942.s001.

Ferreira, L.S., Duarte, D.H.S., 2022. Local climate zone (LCZ) map of the São Paulo metropolitan region - 2010. Mendeley Data V2. https://doi.org/10.17632/48vfvn7v3k.2 (Accessed 22 Sep 2022).
Ferreira, M.J., Oliveira, A.P., Soares, J., 2011. Anthropogenic heat in the City of São Paulo, Brazil. Theor. Appl. Climatol. 104, 43–56. https://doi.org/10.1007/s00704-010-0322-7.
Ferreira, M.J., Oliveira, A.P., Soares, J., Codato, G., Barbaro, E.W., Escobedo, J.F., 2012. Radiation balance at the surface in the city of São Paulo, Brazil: diurnal and seasonal variations. Theor. Appl. Climatol. 107, 229–246. https://doi.org/10.1007/s00704-011-0480-2.
Ferreira, M.J., Oliveira, A.P., Soares, J., 2013. Diurnal variation in stored energy flux in Sao Paulo city, Brazil. Urban Clim. 5, 36–51. https://doi.org/10.1016/j.uclim.2013.06.001.
Foken, T., 1998. Die scheinbar ungeschlossene Energiebilanz am Erdboden - eine Herausforderung an die Experimentelle Meteorologie. Sitzungsberichte Leibniz-Sozietät 24, 131–150.
Foken, T., 2008. The energy balance closure problem: an overview. Ecol. Appl. 18 (6), 1351–1367. https://doi.org/10.1890/06-0922.1.
Foken, T., Oncley, S., 1995. Workshop on instrumental and methodical problems of land-surface flux measurements. Bull. Am. Meteor. Soc. 76, 1191–1193. https://doi.org/10.1175/1520-0477-76.7.1191.
Foken, T., Wimmer, F., Mauder, M., Thomas, C., Liebhetal, C., 2006. Some aspects of the energy balance closure problem. Atmos. Chem. Phys. 6, 4395–4402. https://doi.org/10.5194/acp-6-4395-2006.
Fortuniak, K., Pawlak, W., Siedlecki, M., 2013. Integral turbulence statistic over a central European city Centre. Bound.-Layer Meteorol. 146, 257–276. https://doi.org/10.1007/s10546-012-9762-1.
Fratini, G., Mauder, M., 2014. Towards a consistent eddy-covariance processing: an intercomparison of Eddy-pro and TK3. Atmos. Meas. Tech. 7, 2273–2281. https://doi.org/10.5194/amt-7-2273-2014.
Gao, Z., Liu, H., Katul, G.G., Foken, T., 2017. Non-closure of the surface energy balance explained by phase difference between vertical velocity and scalars of large atmospheric eddies. Environ. Res. Lett. 12 (3) https://doi.org/10.1088/1748-9326/aa625b.
GEOSAMPA, 2020. Portal Geosampa. Secretaria Municipal de Desenvolvimento Urbano. Prefeitura Municipal de São Paulo. Available online *in Portuguese* at. https://tinyurl.com/y6erk5b6 (Accessed 22 Sep 2022).
Goldbach, A., Kuttler, W., 2013. Quantification of turbulent heat fluxes for adaptation strategies within urban planning. Int. J. Climatol. 33 (1), 143–159. https://doi.org/10.1002/joc.3437.
Grimmond, C.S.B., 1992. The suburban energy balance: methodological considerations and results for a mid-latitude west coast city under winter and spring conditions. Int. J. Climatol. 12 (5), 481–497. https://doi.org/10.1002/joc.3370120506.
Grimmond, C.S.B., Oke, T.R., 1995. Comparison of heat fluxes from Summertimes observations in the suburbs of four north American cities. J. Appl. Meteorol. 34 (4), 873–889. https://doi.org/10.1175/1520-0450(1995)034<0873:COHFFS>2.0.CO;2.
Grimmond, C.S.B., Oke, T.R., 1999. Heat storage in urban areas: local-scale observations and evaluation of a simple model. J. Appl. Meteorol. 38 (7), 922–940. https://doi.org/10.1175/1520-0450(1999)038<0922:HSIUAL>2.0.CO;2.
Grimmond, C.S.B., Cleugh, H.A., Oke, T.R., 1991. An objective heat storage model and its comparison with other schemes. Atmos. Environ. Part B Urban Atmos. 25 (3), 311–326. https://doi.org/10.1016/0957-1272(91)90003-W.
Grimmond, C.S.B., Roth, M., Oke, T.R., Au, Y.C., Best, M., Betts, R., Carmichael, G., Cleugh, H., Dabberdt, W., Emmanuel, R., Freitas, E., Fortuniak, K., Hanna, S., Klein, P., Kalkstein, L.S., Liu, C.H., Nickson, A., Pearlmutter, D., Sailor, D., Voogt, J., 2010. Climate and more sustainable cities: climate information for improved planning and Management of Cities (producers/capabilities perspective). Procedia Environ. Sci. 1, 247–274. https://doi.org/10.1016/j.proenv.2010.09.016.
Hao, L., Huang, X., Qin, M., Liu, Y., Li, W., Sun, G., 2018. Ecohydrological processes explain urban dry island effects in a wet region, southern China. Water Resour. Res. 54, 6757–6771. https://doi.org/10.1029/2018WR023002.
IBGE, 2018. Available online at. http://www.ibge.gov.br/english/ (Accessed 22 Sep 2022).
Jog, S., Dixit, M., 2016. Supervised classification of satellite images. In: 2016 Conference on Advances in Signal Processing (CASP), pp. 93–98. https://doi.org/10.1109/CASP.2016.7746144.
Kljun, N., Calanca, P., Rotach, M.W., Schmid, H.P., 2015. A simple two–dimensional parameterization for flux footprint prediction (FFP). Geosci. Model Dev. 8, 3695–3713. https://doi.org/10.5194/gmd-8-3695-2015.
Kormann, R., Meixner, F.X., 2001. An analytical footprint model for non-neutral stratification. Bound.-Layer Meteorol. 99, 207–224. https://doi.org/10.1023/A:1018991015119.
Landsberg, H.E., 1981. The Urban Climate. In: International Geophysics Series, vol. 28. Academic Press, New York-NY, 278 pp.
Leclerc, M.Y., Foken, T., 2014. Footprints in Micrometeorology and Ecology. Springer Berlin, Heidelberg, 239 pp.
Leuning, R., van Gorsel, E., Massman, W.J., Isaac, P.R., 2012. Reflections on the surface energy imbalance problem. Agric. For. Meteorol. 156, 65–74. https://doi.org/10.1016/j.agrformet.2011.12.002.
Majozi, N.P., Mannaerts, C.M., Ramoelo, A., Mathieu, R., Nickless, A., Verhoef, W., 2017. Analysing surface energy balance closure and partitioning over a semi-arid savanna FLUXNET site in Skukuza, Kruger National Park, South Africa. Hydrol. Earth Syst. Sci. 21, 3401–3415. https://doi.org/10.5194/hess-21-3401-2017.
Masseroni, D., Corbari, C., Mancini, M., 2014. Limitations and improvements of the energy balance closure with reference to experimental data measured over a maize field. Atmósfera 27 (4), 335–352. https://doi.org/10.1016/S0187-6236(14)70033-5.
Mauder, M., Foken, T., Cuxart, J., 2020. Surface-energy-balance closure over land: a review. Bound.-Layer Meteorol. 177, 395–426. https://doi.org/10.1007/s10546-020-00529-6.
Meyn, S.K., Oke, T.R., 2009. Heat fluxes through roofs and their relevance to estimates of urban heat storage. Energ. Buildings 41 (7), 745–752. https://doi.org/10.1016/j.enbuild.2009.02.005.
Mohajerani, A., Bakaric, J., Jeffrey-Bailey, T., 2017. The urban heat island effect, its causes, and mitigation, with reference to the thermal properties of asphalt concrete. J. Environ. Manag. 197, 522–538. https://doi.org/10.1016/j.jenvman.2017.03.095.
Moreira, G.A., Oliveira, A.P., Codato, G., Sánchez, M.P., Tito, J.V., Silva, L.A.H., Silveira, L.C., Silva, J.J., Lopes, F.J.S., Landulfo, E., 2022b. Assessing spatial variation of PBL height and aerosol layer aloft in São Paulo megacity using simultaneously two Lidar during winter 2019. Atmosphere 13 (4), 611. https://doi.org/10.3390/atmos13040611.
Moreira, G.A., Oliveira, A.P., Sánchez, M.P., Codato, G., Lopes, F.J.S., Landulfo, E., Marques Filho, E.P., 2022a. Performance assessment of aerosol-lidar remote sensing skills to retrieve the time evolution of the urban boundary layer height in the Metropolitan Region of São Paulo City, Brazil. Atmos. Res. 277 https://doi.org/10.1016/j.atmosres.2022.106290.
Moriwaki, R., Kanda, M., 2004. Seasonal and diurnal fluxes of radiation, heat, water vapor, and carbon dioxide over a suburban area. J. Appl. Meteorol. 43 (11), 1700–1710. https://doi.org/10.1175/JAM2153.1.
Neftel, A., Spirig, C., Ammann, C., 2008. Application and test of a simple tool for operational footprint evaluations. Environ. Pollut. 152, 644–652. https://doi.org/10.1016/j.envpol.2007.06.062.
Ng, E., et al., 2012. A study on the cooling effects of greening in a high-density city: an experience from Hong Kong. Build. Environ. 47 (1), 256–271. https://doi.org/10.1016/j.buildenv.2011.07.014.
Offerle, B., Grimmond, C.S.B., Fortuniak, K., 2005. Heat storage and anthropogenic energy flux in relation to the energy balance of a central European city Centre. Int. J. Climatol. 25 (10), 1405–1419. https://doi.org/10.1002/joc.1198.
Oke, T.R., 1982. The energetic basis of the urban Heat Island. Q. J. R. Meteorol. Soc. 108, 1–24. https://doi.org/10.1002/qj.49710845502.
Oke, T.R., 1988. The urban energy balance. Prog. Phys. Geogr. 12 (4), 471–508. https://doi.org/10.1177/030913338801200401.
Oke, T.R., Cleugh, H.A., 1987. Urban heat storage derived as energy budget residuals. Bound.-Layer Meteorol. 39, 233–245. https://doi.org/10.1007/BF00116120.
Oliphant, A.J., Grimmond, C.S.B., Zutter, H.N., Schmid, H.P., Su, H.B., Scott, S.L., Offerle, B., Randolph, J.C., Ehman, J., 2004. Heat storage and energy balance fluxes for a temperate deciduous forest. Agric. For. Meteorol. 126 (3–4), 185–201. https://doi.org/10.1016/j.agrformet.2004.07.003.

Oliveira, A.P., Marques Filho, E.P., Ferreira, M.J., Codato, G., Ribeiro, F.N.D., Landulfo, E., Moreira, G.A., et al., 2020. Assessing urban effects on the climate of metropolitan regions of Brazil - preliminary results of the MCITY BRAZIL project. Explor. Envir. Sci. Res. 1 (1), 38–77.

O'Malley, C., Piroozfar, P., Farr, E.R., Pomponi, F., 2015. Urban Heat Island (UHI) mitigating strategies: a case-based comparative analysis. Sustain. Cities Soc. 19, 222–235. https://doi.org/10.1016/j.scs.2015.05.009.

Oncley, S.P., Foken, T., Vogt, R., Kohsiek, W., DeBruin, H.A.R., Bernhofer, C., Christen, A., et al., 2007. The energy balance experiment EBEX-2000. Part I: overview and energy balance. Bound.-Layer Meteorol. 123 (1), 1–28. https://doi.org/10.1007/s10546-007-9161-1.

Ribeiro, F.N.D., Oliveira, A.P., Soares, J., Miranda, R.M., Barlage, M., Chen, F., 2018. Effect of sea breeze propagation on the urban boundary layer of the metropolitan region of Sao Paulo, Brazil. Atmos. Res. 214 (June), 174–188. https://doi.org/10.1016/j.atmosres.2018.07.015.

Rizwan, A.M., Dennis, Y.C., Liu, C., 2008. A review on the generation, determination and mitigation of urban heat island. J. Environ. Sci. 20 (1), 120–128. https://doi.org/10.1016/S1001-0742(08)60019-4.

Roth, M., 2007. Review of urban climate research in (sub) tropical regions. Int. J. Climatol. 27, 1859–1873. https://doi.org/10.1002/joc.1591.

Sailor, D.J., Georgescu, M., Milne, J.M., Hart, M.A., 2015. Development of a National Anthropogenic Heating Database with an extrapolation for international cities. Atmos. Environ. 118, 7–18. https://doi.org/10.1016/j.atmosenv.2015.07.016.

Sánchez, M.P., Oliveira, A.P., Varona, R.P., Tito, J.V., Codato, G., Ribeiro, F.N.D., Marques Filho, E.P., Silveira, L.C., 2020. Rawinsonde-based analysis of the urban boundary layer in the metropolitan region of São Paulo, Brazil. Earth Space Sci. 7 https://doi.org/10.1029/2019EA000781 e2019EA000781.

Sánchez, M.P., Oliveira, A.P., Varona, R.P., Tito, J.V., Codato, G., Ynoue, R.Y., Ribeiro, F.N.D., Marques Filho, E.P., Silveira, L.C., 2022. Observational investigation of the low-level jets in the metropolitan region of São Paulo, Brazil. Earth Space Sci. 9, e2021EA002190 https://doi.org/10.1029/2021EA002190.

Schalkwijk, J., Jonker, H.J.J., Siebesma, A.P., 2016. An investigation of the Eddy-covariance flux imbalance in a year-long large-Eddy simulation of the weather at Cabauw. Bound.-Layer Meteorol. 160, 17–39. https://doi.org/10.1007/s10546-016-0138-9.

Shahmohamadi, P., Che-Ani, A.I., Maulud, K.N.A., Tawil, N.M., Abdullah, N.A.G., 2011. The impact of anthropogenic heat on formation of urban Heat Island and energy consumption balance. Urban Stud. Res. 2011, 1–9. https://doi.org/10.1155/2011/497524.

Shepherd, J.M., 2013. Impacts of urbanization on precipitation and storms: physical insights and vulnerabilities. In: Climate Vulnerability: Understanding and Addressing Threats to Essential Resources, vol. 5. Elsevier. https://doi.org/10.1016/B978-0-12-384703-4.00503-7.

Silveira, L.C., Oliveira, A.P., Sánchez, M.P., Codato, G., Ferreira, M.J., Marques Filho, E.P., Božnar, M.Z., Mlakar, P., 2022. Observational investigation of the statistical properties of surface-layer turbulence in a suburban area of São Paulo, Brazil: objective analysis of scaling-parameter accuracy and uncertainties. Bound.-Layer Meteorol. https://doi.org/10.1007/s10546-022-00726-5.

Sokhi, R.S., Francis, X., Kong, X., Miranda, A., Matthias, V., Schere, K., 2018. Basic concepts of mesoscale modelling for air pollution applications. In: Sokhi, R., Baklanov, A., Schlünzen, K. (Eds.), Mesoscale Modelling for Meteorological and Air Pollution Applications. Anthem Press. Available online at, New York, NY, pp. 7–40. https://doi.org/10.2307/j.ctv80cdh5 (Accessed 22 Sep 2022).

Stewart, I.D., Oke, T.R., 2012. Local climate zones for urban temperature studies. Bull. Am. Meteor. Soc. 93 (12), 1879–1900. https://doi.org/10.1175/BAMS-D-11-00019.1.

Taha, H., 1997. Urban climates and heat islands: albedo, evapotranspiration, and anthropogenic heat. Energ. Buildings 25 (2), 99–103. https://doi.org/10.1016/S0378-7788(96)00999-1.

Templeton, N., Vivoni, E., Wang, Z.H., Schreiner-Mcgraw, A., 2018. Quantifying water and energy fluxes over different urban land covers in Phoenix, Arizona: water and energy fluxes over urban cover. J. Geophys. Res. Atmos. 123 (4), 2111–2128. https://doi.org/10.1002/2017JD027845.

Torres, F.D.R., de Oliveira, A.P., da Silveira, L.C., 2023. Sensible, latent heat and store energy fluxes in the suburban São Paulo megacity: seasonal and interannual variations and empirical modeling. Int. J. Hydro. 7 (4), 151–158. https://doi.org/10.15406/ijh.2023.07.00351.

Umezaki, A.S., Ribeiro, F.N.D., Oliveira, A.P., Soares, J., Miranda, R.M., 2020. Numerical characterization of spatial and temporal evolution of summer urban heat island intensity in São Paulo, Brazil. Urban Clim. 32 (March), 100615 https://doi.org/10.1016/j.uclim.2020.100615.

UN, 2016. The World's Cities in 2016. Data Booklet (ST/ESA/ SER.A/392), New York, USA, 29p. Available online at: https://tinyurl.com/y2q4xa9t (Accessed 22 Sep 2022).

UN, 2018. Department of Economic and Social Affairs, Population Division (2018). The World's Cities in 2018-Data Booklet (ST/ESA/ SER.A/417), 34p. Available online at: https://www.un.org/development/desa/pd/sites/www.un.org.development.desa.pd/files/files/documents/2020/Jan/un_2018_worldcities_databooklet.pdf (Accessed 22 Sep 2022).

Wilson, K., Goldstein, A., Falge, E., Aubinet, M., Baldocchi, D., Berbigier, P., Bernhofer, C., Ceulemans, R., Dolman, H., Field, C., Grelle, A., Ibrom, A., Law, B.E., Kowalski, A., Meyers, T., Moncrieff, J., Monson, R., Oechel, W., Tenhunen, J., Valentini, R., Verma, S., 2002. Energy balance closure at FLUXNET sites. Agric. For. Meteorol. 113 (1–4), 223–243. https://doi.org/10.1016/S0168-1923(02)00109-0.

Yang, Q., Su, W., Lin, Z., 2022. A microclimate model for plant transpiration effects. Urban Clim. 45, 101240 https://doi.org/10.1016/j.uclim.2022.101240.

Zhang, K., Chui, T.F.M., 2019. Linking hydrological and bioecological benefits of green infrastructures across spatial scales – a literature review. Sci. Total Environ. 646, 1219–1231. https://doi.org/10.1016/j.scitotenv.2018.07.355.

Zhou, Y., Li, D., Liu, H., Li, X., 2018. Diurnal variations of the flux imbalance over homogeneous and heterogeneous landscapes. Bound.-Layer Meteorol. 168, 417–442. https://doi.org/10.1007/s10546-018-0358-2.

Zhou, Y., Li, D., Li, X., 2019. The effects of surface heterogeneity scale on the flux imbalance under free convection. J. Geophys. Res. Atmos. 124 (15), 8424–8448. https://doi.org/10.1029/2018JD029550.